

Ryan Honeyager*, Guosheng Liu, Holly Nowell
Florida State University, Tallahassee, FL

1. Introduction

Microwave radar and radiometers greatly facilitate observations of cloud processes. Cirrus clouds are predominantly comprised of solid ice hydrometeors. Unlike with liquid water, ice particles are solid, and thus may form many different shapes. Small changes in particle shape can have a great impact on overall scattering behavior, as hydrometeor size is of the same order of magnitude as the wavelength of microwave radiation.

Many studies have modeled ice particles using idealized particle shapes, such as spheres, oblate and prolate ellipsoids, hexagonal plates, sector snowflakes, dendrites, and bullet rosettes. These shapes generally possess one or more degrees of symmetry. However, these idealized morphologies match only a relatively small fraction of observed particles [Korolev and Isaac 2003]. Prior field campaigns have indicated that ice crystals are more commonly-observed to be comprised of aggregates of smaller crystals [Westbrook et al. 2004], and attempts to approximate these aggregates by using simpler particles along with any form of effective medium approximation provides poor results. For example, Kim [2006] used the discrete dipole approximation to compute single scattering properties of simple columnar aggregates and established that Mie theory did not adequately predict single-scattering properties, such as asymmetry factor (g), scattering (C_{sca}) and absorption cross-sections (C_{abs}) for size parameters greater than 2.5. Here, size parameter is defined as $\chi=2\pi\cdot a_{eff}/\lambda$, where λ is the wavelength of incident light, and a_{eff} is the effective radius of a given particle. Effective radius is defined as the radius of an equivalent solid ice-volume sphere.

Aggregate formulations have been proposed using bullet rosettes [Westbrook et al. 2006; Nowell et al. 2013], planar dendritic snowflakes [Petty and

Huang 2010], stellar-type crystals [Botta et al. 2011] and spheres [Maruyama and Fujiyoshi 2005]. Given the complexity of aggregate flakes, the discrete dipole approximation [Draine and Flatau 2012] and Rayleigh-Gans approximation [Hogan and Westbrook 2014] are commonly used. Significant deviations from T-matrix theory using a Maxwell-Garnett and Sihvola effective medium approximations [Maxwell Garnett 1904; Bohren and Huffman 1983; Sihvola 1989] was observed in Petty and Huang [2010], Honeyager [2013] and Nowell et al. [2013]. The largest deviations were observed in the differential scattering cross-section at exact backscatter direction (herein defined as backscatter), where the differences over different particle morphologies (dendrites, aggregates, rosettes) and solution methods (DDA, T-matrix) varied by up to several orders of magnitude [Nowell et al. 2013; Honeyager 2013; Tyynelä et al. 2011; Petty and Huang 2010]. As the differential backscatter cross-section over a particle ensemble is used in the radar reflectivity relation, accurate knowledge of backscatter is essential.

These pristine flake and aggregate reconstructions are all based on observational studies that usually consist single- or multi-angle imagery of many individual particles [Garrett 2012; Hanesch 1999; Korolev and Issac 2003], sometimes combined with a measure of particle mass. These measurements provide some knowledge about aspect ratio (AR), fractal dimension (f_d) and about the mass / density relationship. However, near same-mass aggregates with near-matching measurements of these above quantities still can vary considerably in backscatter and scattering cross-section [Nowell et al. 2013]. Relative uncertainty in backscatter and scattering cross-section were found to vary by up to 30%. Between different aspect-ratio aggregates, there was considerable overlap in single-scattering properties, but the relative uncertainty increased to near an order of magnitude. It should also be noted that these methods attempt to model aggregates based solely on knowledge of surface features + overall mass. There are few constraints on the ‘interior’ of these particles, which increases uncertainty

* *Corresponding author address:* Ryan Honeyager, Florida State University, Dept. of Earth, Ocean and Atmospheric Science, Tallahassee, FL 32306-4520; e-mail: rhoneyager@fsu.edu

about the physicality of such results.

In this paper, we examine how backscatter is impacted by surface and interior features. Aggregates have a complex structure, consisting of many void-like regions filled with air along with a pseudorandom ice structure. We develop an algorithm to determine the effective surface area and volume of these particles, and further use this algorithm to separate the relative contributions of interior versus exterior structural features on the particle's overall single-scattering properties. As the interior structure is hard to measure, we use this approach to determine lower bounds of uncertainty in scattering behavior.

2. Aggregate Database

We used Nowell [2010] and Nowell et al. [2013] to provide a base database of aggregates. These aggregates are grown from chains of 6-bullet rosettes (Figure 2). In cirrus clouds, bullet rosettes tend to have maximal dimensions between 200 and 800 microns [Pruppacher and Klett 1997] and follow a range of size-density relationships. In this study, the “bullets” in the rosettes are assumed to be columns made of equal-sized cubes with orthogonally oriented columns that share the same single cube in the center (Figure 1). As the size-density relationship for bullet rosettes in Heymsfield et al. [2002] closely matched the calculated densities of our base rosettes with maximum dimensions of 200 and 400 microns, we used these as the base rosettes for aggregate generation (Figure 3). Three cases were considered when constructing aggregates: 200 micron base rosettes only, 400 micron base rosettes, and aggregates constructed using both rosette sizes.

The bullet rosettes are randomly-placed, with each subsequent bullet rosette in the chain being placed somewhere adjacent to the previous rosette. Bullet rosettes are not allowed to intersect. Chains of rosettes are grown until there is no more room for expansion of the chain or until the chain reaches predefined bounds on overall particle diameter. The final aggregates (example in Figure 2) are modeled to match previous observations of aggregate aspect ratios, fractal dimension and mass-density relationship. Runs were conducted at 263 K at several frequencies ranging from 3 to 183.31 GHz.

Three different aspect ratio parameterizations

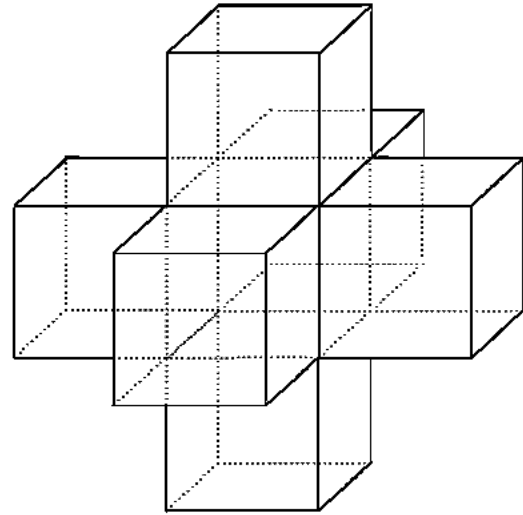
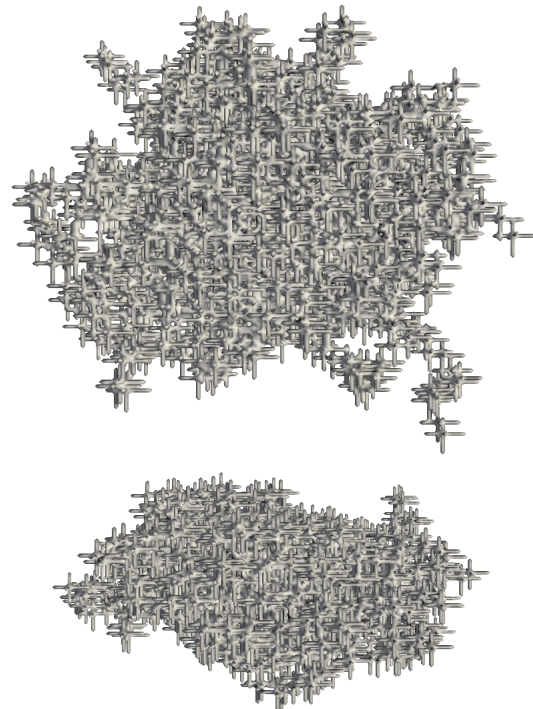


Figure 1 - A 6-bullet rosette used in aggregate construction in Nowell et al. [2013].

Figure 2 - Example AR 0.6 oblate aggregate, with top and size views.



are considered: spheroidal, oblate and prolate aggregates. The spheroidal aggregates [Nowell 2010] are approximately round, with aspect ratios near 0.8-1.0. These are based on observations from Magono and Nakamura [1965] and Brandes et al. [2007]. 557 aggregates were generated, with effective radii from 180 to 1460 μm , and maximum diameters from 765 to 12,585 μm . Oblate aggregates resemble flattened spheroids, with aspect ratios near 0.6. These correspond to observations from Korolev and Issac [2003]. There are 240 oblate aggregates. Additionally, a new parameterization for prolate aggregates (similar to elongated spheroids) is considered to also match Korolev and Issac [2003], with aspect ratios also near 0.6. 180 prolate aggregates were generated.

Fractal dimension, d_f , was also constrained to match prior studies. Fractal dimension is a representation of how fast the volume changes as a function of the total diameter. The relationship between fractal dimension, mass (or volume) and linear diameter is $M = a \cdot r^{d_f}$, where M is the mass of the aggregate, r is the effective radius and a is a scaling constant [Westbrook et al. 2004]. The scaling constant depends on the method used to determine the other parameters. Muramoto et al. [1993] used a divider method, in which only the outline of flake images was used in determining d_f . In contrast, Maruyama and Fujiyoshi [2005] and Ishimo-

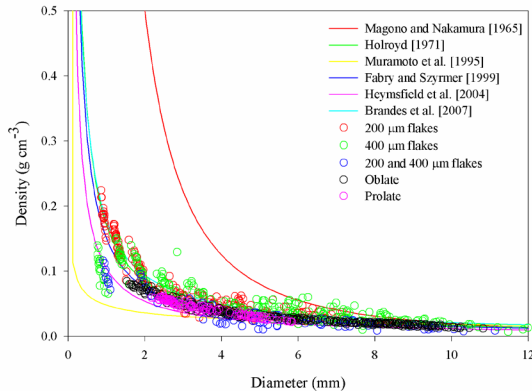


Figure 3 - Size-density relationships from Brandes et al. [2007], plotted against the aggregates considered in this study. Randomly generated AR 0.8 flakes are divided into 200, 400 and 200 and 400 μm flakes as red, green and blue circles, respectively. Oblate (AR 0.6) and prolate flakes are shown as black and pink circles, respectively.

to [2008] used a box counting method, where the entire filled flake image was examined. The aggregates generated in this study have an outline d_f of 1.29 and a full-image d_f of 1.75, respectively matching the above definitions.

The overall size-density relationship for the aggregates was constrained to roughly follow the Brandes et al. [2007] diameter-density relationship. Deviations from this relation up to 20% were allowed, to correspond to results from other observational studies [Magono and Nakamura 1965; Holroyd 1971, Muramoto et al. 1995; Fabry and Szyrmer 1999; Heymsfield et al. 2004].

For comparison, this aggregate database is supplemented with pristine flake results from Liu [2004; 2008]. The morphologies considered include dendrite snowflakes and sector snowflakes. These particles are solid. They have well-defined ice interiors and exteriors, and have uniquely and clearly-defined surface areas and volumes.

3. Single-Scattering Approximation

The single-scattering properties were calculated using the discrete dipole approximations [Draine 1988]. The scattering, absorption and differential backscatter cross-sections were calculated, as well as the asymmetry parameter. The quantities were then normalized by a factor of $\pi \cdot a_{\text{eff}}^2$ to produce normalized cross-sections ($C_{\text{sca}} / \pi \cdot a_{\text{eff}}^2 = Q_{\text{sca}}$, $C_{\text{abs}} \rightarrow Q_{\text{abs}}$, etc.), which are shown in Figure 4. The ice particles are represented as an array of polarizable cells on a cubic lattice. The interdipole spacing for the aggregates is either 40 or 57.1 microns, corresponding to the use of either 200 or a 400 micron bullet rosettes as the aggregate base. This small interdipole spacing ensures that the DDA converges. The number of dipoles used in modeling varied from 134 to 160,301. All calculations are done assuming random particle orientation.

Results are shown in Figure 4. The solid ice spheroid approximation is a poor fit for these aggregates. Significant deviations with aggregate results are already present at $\chi = 1$ for Q_{abs} and Q_{sca} . The aggregate results do not show the resonance effects commonly observed in spheroids [Zubko et al. 2010], as these aggregates have neither a symmetric nor smooth surface. Q_{sca} for aggregates is larger than the solid sphere results, indicating that the aggregates attenuate more light by scattering processes. However, spheres backscatter more

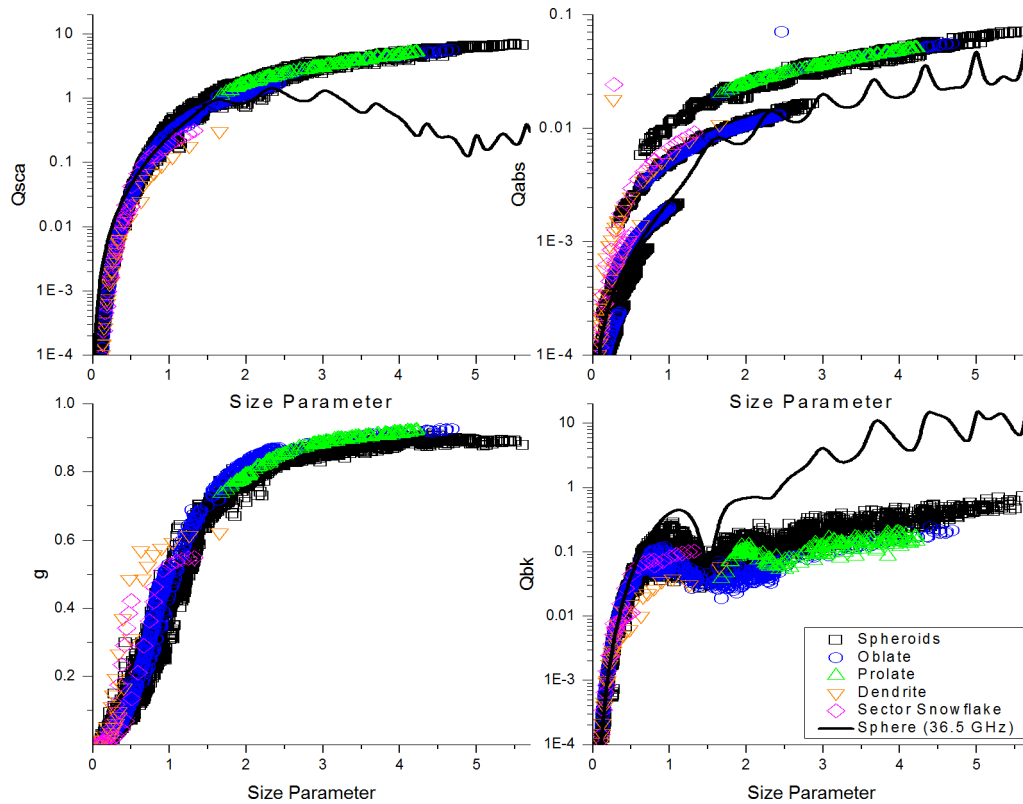


Figure 4 - Plot of the single-scattering properties for aggregate flakes and Liu [2008] snowflakes. Different flake morphologies are shown in different colors. Solid spheres at 36.5 GHz are shown as the solid line.

light than aggregates do. Aggregates absorb more light than equivalent-mass spheres.

Differences in aggregate aspect ratio led to pronounced differences in Q_{bk} . Backscatter varies by up to an order of magnitude among spheroids, oblate and prolate aggregates. Oblate and prolate flakes show markedly lower backscatter than spheroids. Similar differences are also observed in Q_{sca} , though the degree of difference is less pronounced. Q_{abs} and g are nearly identical for different aggregate morphologies.

4. Defining an Effective Surface

As mentioned in the previous section, there is a large variation in backscatter cross-section even when particles are constrained by aspect ratio,

and AR 0.6 oblate and prolate aggregates exhibit lower values of backscatter when compared with near-spheroidal AR 0.8 aggregates. The aggregates are composed of bullet rosettes and contain a diffuse ice lattice that is heavily filled with air. As such, these particles have an ill-defined surface area and volume. As these particles have features that vary at scales smaller than microwave radar wavelengths, it would be convenient to define a consistent 'effective volume' and 'effective surface area' for each hydrometeor.

We used a Voronoi cell-based approach to define these quantities. The term 'effective' in both effective volume and surface area is used in the same sense as when used in determining an effective dielectric for Mie and T-Matrix-based computations. Voronoi cells [Rycroft 2009] are constructed

around each of the ice lattice points in our flakes. The volume contained within each specific cell is the region of space that is closest to a specific ice lattice point. We use this approach for several reasons: 1) the surface of all of the Voronoi cells has features that vary on the micron and millimeter scale, 2) the resultant surface follows the contours of the base aggregate that it is generated from, unlike in a convex ellipsoid of circumscribing sphere-based approach [Honeyager 2013] and 3) that the volume fraction of solid ice to total enclosed volume is substantially different from $f_{ice}/f_{total} \approx 0$. This final feature allows for good comparisons with effective dielectric medium approximations. This approach produces a consistent definition of effective surface area and volume. The surface of each aggregate is closed and has an easily-calculable surface area (Figure 6). As expected, the effective surface area and volume increase with increasing hydrometeor

mass.

The surface area (SA) to volume (V) ratio can be used as a measure of the surface roughness and complexity of each particle. For a given particle mass, the minimum possible ratio of SA/V occurs for the solid ice sphere case. For spheres, the ratio then is $3/R$, where R is the sphere radius. This minimum changes with particle size and has units of inverse length. For a consistent comparison of particles of different mass, we normalize the SA/V ratio of selected hydrometeors against the SA/V ratio of the equivalent-mass solid sphere. For this normalized quantity, a SA/V index of 1 corresponds always to a solid sphere case. All other values correspond to a greater surface area for the same particle mass, indicating a more complex shape. Figure 7 shows the backscatter results for AR 0.6 oblate and prolate aggregates, AR 0.8 aggregates, and select dendritic and sector snowflakes over

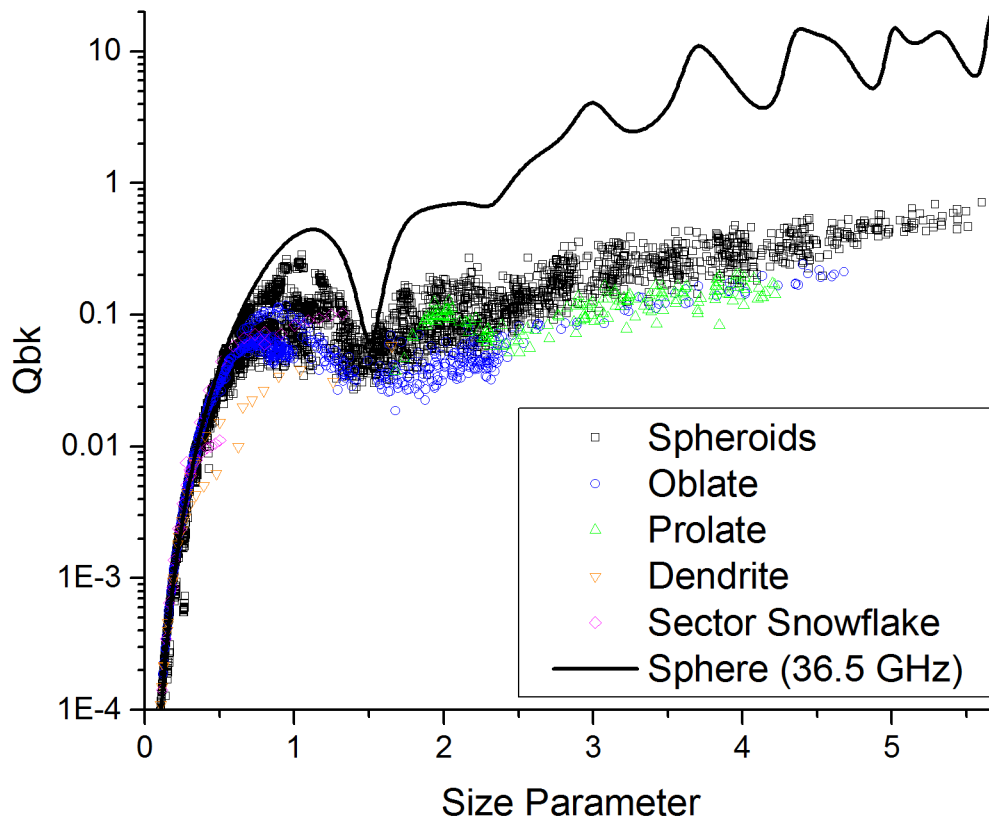


Figure 5 - Expanded view of the plot of backscatter in Figure 4.

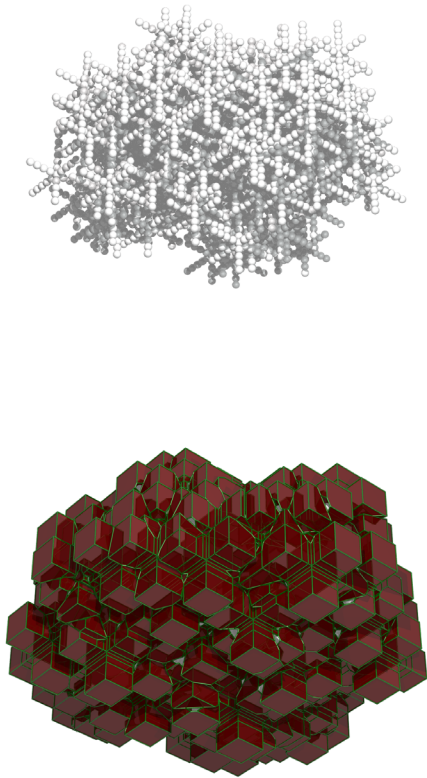


Figure 6 - Example oblate aggregate, showing the underlying filled ice dipoles (above) and the Voronoi-determined surface (below). The initial flake has an ill-defined surface area and volume. It lacks a clearly-defined interior and exterior. The Voronoi surface has none of these limitations.

several frequencies from 36.5 to 183.31 GHz. Each point is colored according to that particle's normalized SA/V ratio. Scattering cross-section results are visible in Figure 8. The cross-sectional results for a solid ice sphere at 36.5 GHz are plotted for reference. For all particle masses, the results show a consistent and well-defined trend where a greater surface complexity leads to a lower backscatter. This is expected physically, as a more complex surface is less likely to backscatter radiation, but this contouring of points quantifies this relationship. The results in Figure 7 may be compared against those in Figure 5, which only filters flakes based on aspect ratio.

5. Interior Perturbations

The same Voronoi technique can be applied to the interior of a hydrometeor. We separated each particle into surface and interior components, with the interior defined as all lattice sites further than two Voronoi cells away from the Voronoi-defined surface of the particle (Figure 9). Hydrometeor imaging studies provide no knowledge of particle interiors, other than an occasional rough estimate of particle mass. So, we examine sensitivity to internal features by perturbing the particle interior. Overall particle mass is preserved, while the interior lattice sites are all randomized. This represents a situation where all information of the particle interior has been lost, yet it preserves the large number of internal reflections of light through the ice / void lattice. This internal scattering is neglected in many non-DDA formulations that use an effective medium approximation [Draine and Goodman 1993; Kim 2006; Zubko et al. 2010].

AR 0.6 oblate aggregates at 36.5, 89 and 183.31 GHz were perturbed this way. The structured interior (original) vs. unstructured (perturbed) comparison is shown in Figure 10. Each original and perturbed point pair has the same mass, so these points all lie on the same vertical line. The percent change in backscatter varied based on frequency. Worst case results occurred at 183.31 GHz, where the mean percent difference between perturbed and original results was under 20%. For lower frequencies, such as 36.5 GHz, the average percent difference was 12%. The mean percent change in scattering cross-section was under 2%. The randomized interior cases did have a consistently lower backscatter than the initial aggregates. The randomized interior lattice varies randomly on the scale on a single dipole spacing, so an accurate backscatter calculation is expected to be somewhat unreliable at this resolution [Zubko et al. 2010]. Overall, these results show that knowledge of interior structure is less critical than accurately representing particle surface, and that with surface area, volume and mass, it is possible to predict the microwave backscatter and other cross-sections with good accuracy.

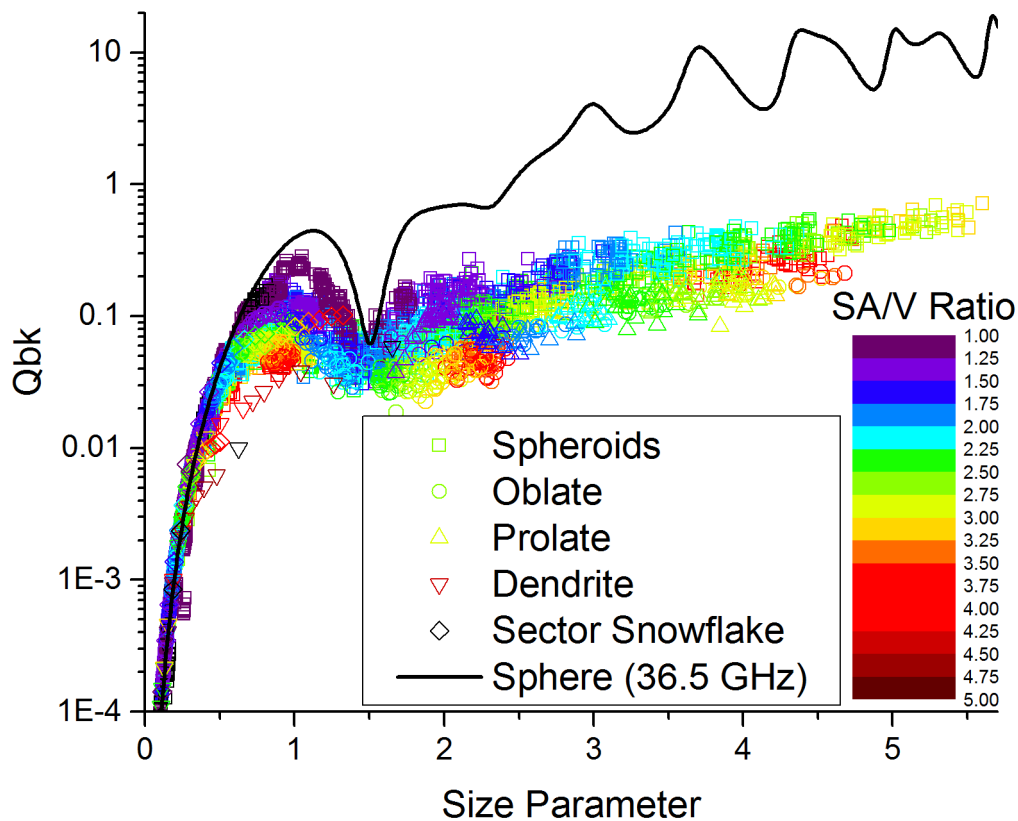


Figure 7 - Backscatter plot (refer to Figure 5), but coloring based on Voronoi surface area to volume ratio, normalized against that of a same-mass sphere. Key: AR 0.8 spheroids (squares), AR 0.6 oblate (circles), prolate spheroids (triangles), dendrites (downward-facing triangles), and sector snowflakes (diamonds).

6. Conclusions and Further Work

Three related aggregate models were used to examine trends in single-scattering properties as a function of aspect ratio, mass, frequency and the effects of interior / exterior perturbations on the aggregate lattice structure. Ice crystals with the same mass can vary in backscatter by up to an order of magnitude. The cause of this variation is particle shape (morphology). By constraining flake populations based on aspect ratio, it is possible to lower the uncertainty inherent in backscatter and scattering cross sections. Oblate and prolate (AR 0.6) aggregates show consistently lower backscatter than more spheroidal (AR 0.8-0.9) aggregates. This is caused by the complexity of the aggregate

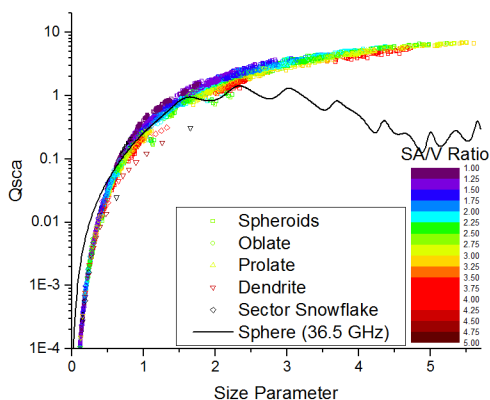


Figure 8 - Scattering cross-section, colored in the same manner as Figure 7.

surface, and deviations from spherical shape lead to lower backscatter. We were able to quantify this by defining an effective surface area and volume using a Voronoi cell-based method, which when combined with aspect ratio can lower uncertainty in backscatter to within a few percent. Stability testing was performed by perturbing aggregate interiors, and interior scattering effects had lower magnitude and thus a smaller contribution to overall backscatter relative to surface-based effects.

These results are important because they validate the feasibility of modeling snowflakes based on observational studies. A measure of particle surface area and mass is recommended in future field campaigns, in addition to the existing measures of aspect ratio, fractal dimension and size-density relation. This study finds a minimum uncertainty in backscatter of around 12% and a minimum uncertainty of 2% in scattering cross-section for modeled results. Further anticipated work will involve comparisons with the T-matrix and Rayleigh-Gans methods and effective medium approximation-derived results, as well as the effects of particle align-

ment on microwave remote sensing.

7. References

- Brandes, E. A., K. Ikeda, G. Zhang, M. Schönhuber, and R. M. Rasmussen, 2007: A statistical and physical description of hydrometeor distribution in Colorado snowstorms using a video disdrometer. *J. Appl. Meteor. Climo.*, 46, 634-649, doi:10.1175/JAM2489.1.
- Bohren, C. F., and D. R. Huffman, 1983: *Absorption and Scattering of Light by Small Particles*. John Wiley and Sons, 530 pp.
- Botta, G., K. Aydin, J. Verlinde, A. E. Avramov, A. S. Ackerman, A. M. Fridlind, G. M. McFarquhar, and M. Wolde, 2011: Millimeter wave scattering from ice crystals and their aggregates: Comparing cloud model simulations with X- and Ka-band radar measurements. *J. Geophys. Res.*, 116, D00T04, doi:10.1029/2011JD015909.
- Draine, B. T., 1988: The discrete-dipole approximation and its application to interstellar graphite grains. *Astrophys. J.*, 333, 848-872, doi:10.1086/166795.
- Draine, B. T. and J. Goodman, 1993: Beyond Clausius-Mossotti: Wave propagation on a polarizable point lattice and the discrete dipole approximation. *Ap. J.*, 405, 685-697, doi:10.1086/172396.
- Draine, B. T. and P. J. Flatau, 2012: User guide for the discrete dipole approximation code DDSCAT 7.2. URL <http://arxiv.org/abs/1202.3424>.
- Fabry, F., and W. Szyrmer, 1999: Modeling of the melting layer. Part II: Electromagnetic. *Journal of the Atmospheric Sciences*, 56, 3593-3600, doi:10.1175/1520-0469(1999)056<3593%3A-MOTMLP>2.0.CO%3B2.
- Garrett, T. J., C. Fallgatter, K. Shkurko, and D. Howlett, 2012:

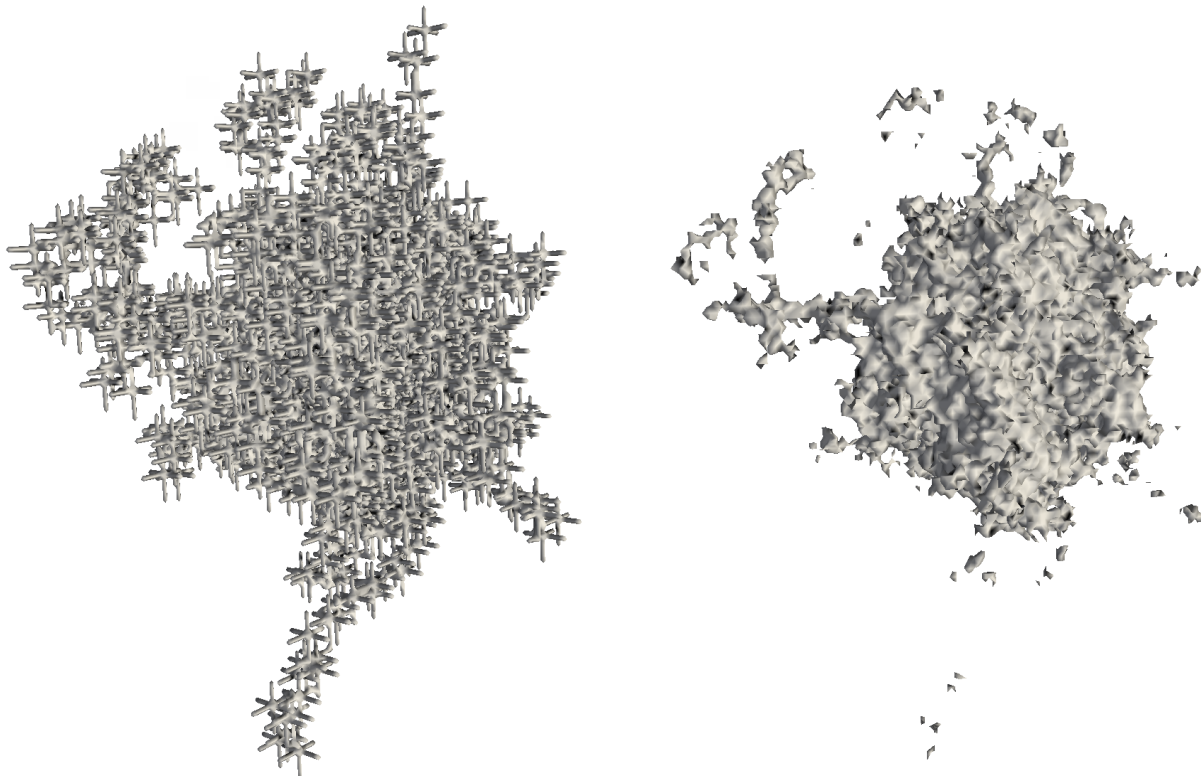


Figure 9 - Voronoi algorithm-determined aggregate surface (left) and contoured interior (right) regions for a sample oblate aggregate. The interior region has a volume fraction of 71% ice.

Fallspeed measurement and high-resolution multi-angle photography of hydrometeors in freefall. *Atmos. Meas. Tech.*, 5, 2625–2633, doi:10.5194/amt-5-2625-2012.

Hanesch, M., 1999: Fall Velocity and Shape of Snowflakes, Ph.D. Dissertation, Swiss Federal Institute of Technology, Zürich, Switzerland.

Heymsfield, A. J., S. Lewis, A. Bansemer, J. Iaquinta, L. M. Miloshevich, M. Kajikawa, C. Twohy, and M. R. Poellot, 2002: A general approach for deriving the properties of cirrus and stratiform ice cloud particles. *J. Atmos. Sci.*, 59(1), 3–29, doi:10.1175/1520-0469(2002)059<0003:AGAFDT>2.0.CO;2.

Heymseld, A. J., A. R. Bansemer, C. G. Schmitt, C. H. Twohy, and M. Poellot, 2004: Effective ice particle densities derived from aircraft data. *J. Atmos. Sci.*, 61, 982–1003, doi:10.1175/1520-0469(2004)061n%3C0982:EIPDDFn%3E2.0.CO;2.

Hogan, R. and C. Westbrook, 2014: Equation for the microwave backscatter cross section of aggregate snowflakes using the Self-Similar Rayleigh-Gans Approximation. *J. Atmos. Sci.*, in press.

Honeyager, R., 2013: Investigating the use of the T-Matrix Method as a Proxy for the Discrete Dipole Approximation, Electronic Theses, Treatises and Dissertations. Paper 7427.

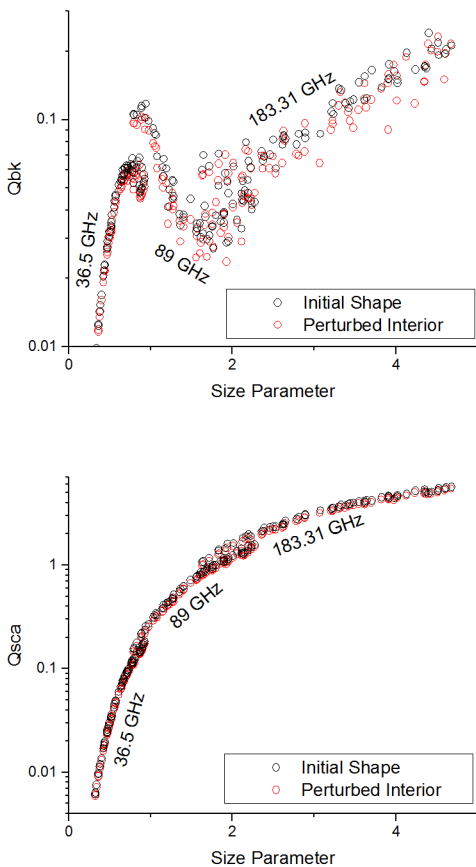


Figure 10 - Backscatter (top) and scattering (bottom) cross-sections for structured (black) and randomized (red) oblate aggregate interiors. Randomized flakes have the same mass as their unperturbed counterparts, so they have the same size parameter (x-axis).

Holroyd, E. W., III, 1971: The meso- and microscale structure of Great Lakes snowstorm bands: A synthesis of ground measurements, radar data, and satellite observations, Ph.D. dissertation, University at Albany, State University of New York, Albany, New York.

Ishimoto, H., 2008: Radar Backscattering Computations for Fractal-Shaped Snowflakes. *J. Meteorol. Soc. Jpn.*, 86(3), 459–469, doi:10.2151/jmsj.86.459.

Kim, M.-J., 2006: Single scattering parameters of randomly oriented snow particles at microwave frequencies. *J. Geophys. Res.*, 111(D14), D14201, doi:10.1029/2005JD006892.

Korolev, A., and G. Isaac, 2003: Roundness and aspect ratio of particles in ice clouds. *J. Atmos. Sci.*, 60(15), 1,795–1,808, doi:10.1175/1520-0469(2003)060<1795:RAAROP>2.0.CO;2.

Liu, G., 2004: Approximation of single scattering properties of ice and snow particles for high microwave frequencies. *J. Atmos. Sci.*, 61(20), 2, 441–2,456, doi:10.1175/1520-0469(2004)061<2441:AOSPO>2.0.CO;2.

Liu, G., 2008: A database of microwave single-scattering properties for nonspherical ice particles. *Bull. Am. Meteorol. Soc.*, 89(10), 1, 563–1,570, doi:10.1175/2008BAMS2486.1.

Magono, C., and T. Nakamura, 1965: Aerodynamic studies of falling snowflakes. *J. Meteorol. Soc. Jpn.*, 43(3), 139–147.

Maruyama, K., and Y. Fujiyoshi, 2005: Monte Carlo simulation of the formation of snowflakes. *J. Atmos. Sci.*, 62(5), 1,529–1,544, doi:10.1175/JAS3416.1.

Maxwell Garnett, J. C., 1904: Colours in metal glasses and in metallic films. *Philos. Trans. Roy. Soc., A*, 203, 385–420.

Muramoto, K., K. Matsuura, and T. Shiina, 1993: Analysis of snowflake shape by a region and contour approach. *Trans. Inst. Electron. Inf. Commun. Eng., Sect. D* (Japanese edition), J76-D-II, 949–958.

Nowell, H. K., 2010: Modeling snow aggregates and their single scattering properties: implications to snowfall remote sensing. M.S. thesis, Florida State University, URL <http://diginole.lib.fsu.edu/etd/2511>, Electronic Theses, Treatises and Dissertations. Paper 2511.

Nowell, H., G. Liu, and R. Honeyager, 2013: Modeling the single-scattering properties of aggregate snowflakes. *J. Geophys. Res. Atmos.*, 118, 7873–7885, doi:10.1002/jgrd.50620.

Petty, G. W., and W. Huang, 2010: Microwave backscatter and extinction by soft ice spheres and complex snow aggregates. *J. Atmos. Sci.*, 67(3), 769–787, doi:10.1175/2009JAS3146.1.

Pruppacher, H. R., and J. D. Klett, 1997: *Microphysics of clouds and precipitation: second revised and enlarged edition with an introduction to cloud chemistry and cloud electricity*, Kluwer Academic Publishers, Norwell, Massachusetts.

Rycroft, C., 2009: Voronoi++: a three-dimensional Voronoi cell library in C++. *Chaos* 19, 041,111.

Sihvola, A. H., 1989: Self-Consistency Aspects of Dielectric Mixing Theories. *IEEE Trans. Geosci. Rem. Sens.*, 27(4), 403–415.

Tyynelä, J., J. Leinonen, D. Moisseev, and T. Nousiainen, 2011: Radar backscattering from snowflakes: comparison of fractal, aggregate, and soft spheroid models. *J. Atmos. Oceanic Tech.*, 28(11), 1,365–1,372, doi:10.1175/JTECH-D-11-00004.1.

Westbrook, C., R. Ball, P. Field, and A. Heymsfield, 2004: Theory of growth by differential sedimentation, with application to snowflake formation. *Phys. Rev. E*, 70(2), 1–7, doi:10.1103/PhysRevE.70.021403.

Westbrook, C. D., R. C. Ball, and P. R. Field, 2006: Radar scattering by aggregate snowflakes. *Q. J. Roy. Meteorol. Soc.*, 132(616), 897–914, doi:10.1256/qj.05.82.

Zubko, E., et al., 2010: Validity criteria of the discrete dipole approximation. *Appl. Opt.*, 49, 1267–1279, doi:10.1364/AO.49.001267.